CBPF-NF-004/95

Density Functional Discrete Variational Study of NH_3 and $NiNH_3$

Joice Terra

Centro Brasileiro de Pesquisas Físicas - CBPF
Rua Dr. Xavier Sigaud, 150
22.290-180 Rio de Janeiro/RJ, Brasil

Abstract

The electronic structures of NH_3 and $NiNH_3$ are investigated by the first-principles Discrete Variational method within on the local spin-density approximation (LSDA) density-functional theory. Calculations were performed to study the total energy as a function of the interatomic distances and to understand the nature of the bonding of lone-pair ligand to transition metal.

Key-words: Ni-ammonia; Bond orders; Total energy.

Introduction

There have been many theoretical investigations about the nature of the bonding lone pair ligands to transition metals [1]. The main interest is related to the fact that important chemical reactions are catalyzed by transition metals. Due to advances in computational techniques more and more problems, like adsorption process of NH_3 on transition metal surfaces [2], have recently been appropriately treated. Bauschlicher and others [1, 3] have extensively studied the mechanism of interaction between several types of ligands to the transition metals by using ab-initio theoretical methods in order to determine the electronic structure [3].

The self-consistent calculation with the Discrete Variational method (DVM) [4] developed in the framework of local spin-density approximation (LSDA) density-functional theory has been successfuly employed to study essentially electronic properties of solids using cluster representation [5]. However, computational schemes for the application of the Density Functional theory to molecular systems have been developed [6].

In the present work we report a study of the NH_3 and $NiNH_3$ molecules using DVM. The nature of the bonding and the energy curves calculated as a function of the interatomic distances are analyzed. Ammonia, for example is a well established system and we can compare the results with those found in current literature. In other words, we are aiming to show that the DVM method can be a reliable scheme to investigate systems with strong directional properties. The theoretical study of the species $FeNH_3$ [7] allows for the interpretation the experimental Mössbauer parameters [8].

Method of Calculation

We have performed electronic structures calculations for the molecules in case, employing the first-principles Discrete Variational method (DVM), developed within the local spin density approximation theory for exchange-correlation energy [9].

The full details of the DVM method have been described elsewhere [4]. The essence of the DVM scheme is to solve the self-consistent one particle Kohn-Sham equations, which for the spin-polarized case [10] are written in Hartree atomic units as:

$$\left[-\frac{1}{2}\nabla^2 + v_{eff}(\vec{r})_\sigma\right]\phi_{i\sigma}(\vec{r}) = \varepsilon_{i\sigma}\phi_{i\sigma} \tag{1}$$

$$v_{eff}(\vec{r})_\sigma = v(\vec{r}) + \int \frac{\rho(\vec{r}\,')}{|\vec{r} - \vec{r}\,'|} d\vec{r}\,' + v_{xc}(\vec{r})_\sigma \tag{2}$$

$$\rho(\vec{r}) = \sum_{i,\sigma} n_{i\sigma} |\phi_{i\sigma}|^2 \qquad i = 1, \cdots, N \tag{3}$$

where the summation in (3) runs over the lowest N molecular spin orbitals $\phi_{i\sigma}$ with occupation $n_{i\sigma}$ which are expanded on a basis of atomic numerical orbitals (LCAO approximation) centered at the symmetrically equivalent atoms. The nuclear attraction and the Coulomb repulsion potentials due to the electrons are described by the first two terms in (2), with $\rho = \rho_\uparrow + \rho_\downarrow$, while the last one is the spin-dependent exchange-correlation. Since both polarized and nonpolarized calculations were made, we have adopted for the exchange-correlation potential in the local-spin-density approximation the one derived by von Barth-Hedin [11], easily adapted to either cases. Whenever the correlation effects are neglected, the von Barth-Hedin potential $v_{xc}(\vec{r})_\sigma$ reduces to the Kohn-Sham potential [11]

$$v_x(\vec{r})_\sigma = -2[3\rho_\sigma(\vec{r})/4\pi]^{1/3} \qquad \text{Hartrees}, \tag{4}$$

where ρ_σ is the density of electrons of spin σ and can be different for the two spin orientations. Both of these potentials were used in our self-consistent calculations in order to observe how far are the results affected by the correlation correction. This correction contains a logarithmic term multiplied by a constant.

The functional dependence of the Coulomb potential on $\rho(\vec{r})$ leads to the so-called three-center integrals, which have a large computational cost. This problem is largely bypassed by DVM, adopting a variational density expansion scheme, which consists of replacing the exact molecular charge density $\rho(\vec{r})$ by a self-consistent multicenter-multipolar (SCM) representation [12]

$$\rho(\vec{r}) \cong \rho_{\mathrm{SCM}}(\vec{r}) = \sum_j d_j \rho_j$$

$$\rho_{\mathrm{j}} = \sum_i^I \sum_m C_{\ell m}^{i\lambda} R_N(r_i) Y_{\ell m}(\vec{r}_i). \tag{5}$$

Here r_i is the local coordinate relative to site i, the i summation is over a symmetry-equivalent set of atoms, the symmetry coefficients $C_{\ell m}^{i\lambda}$ belong to the totally symmetric representation of the molecular point group and R_N are piecewise parabolic radial functions centered on each nucleus i while λ denotes different basis functions of a given ℓ ($j = I, \ell, \lambda, N$). The coefficients d_j are determined numerically by a least-square fit to the charge density on the variational points grid. We have calculated self-consistent results using multipolar densities up to $\ell = 2$ for Ni and N, and $\ell = 1$ for H; the least-square fit leads to errors around 0.02 and 0.06 for $NiNH_3$ and NH_3 respectively.

Besides obtaining the Coulomb potential by one-dimensional numerical integration as desirable, ρ_{SCM} theoretically allows calculations of the Coulomb and exchange-correlation

potentials as precise as one wishes, at the cost of adding more and more terms. It has been verified that ρ_{SCM} is more efficient than anything else to describe the effects of anisotropy bonding charge [12, 13]. That is an important fact whenever systems and properties such as molecules and total energy are investigated.

In the DVM method, the total energy E is calculated by a point by point numerical integration of the difference-energy density [14]

$$E = \langle e(\vec{r}, \{\vec{R}_\nu\}) - e^{NI}(\vec{r}, \{\vec{R}_\nu\})\rangle + E^{NI} \tag{6}$$

in which a reference system of non-interacting (NI) atoms centered at the nucleus sites $\vec{R}_\nu$ is introduced in order to suppress numerical noise arising from the $e(\vec{r}, \{\vec{R}_\nu\})$. The basis set is adopted as the standard reference.

Results and Discussion

A -Some Aspects of the Calculation

The purpose of the present work is to examine the bonding nature and the total energy curves covering a wide range of N-H and Ni-N distances in order to determine the equilibrium distances for NH_3 and $NiNH_3$ respectively. Both of them have C_{3v} structure. For $NiNH_3$, the metal atom is constrained to lie on the main symmetry axis (the z axis) of the ligand. The ammonia in the $NiNH_3$ molecule was treated using the experimental equilibrium geometry [15]: N-H=1.00Å with an angle H-N-H=107.2^0, while it was reasonable to assume that the Ni-N distance is given approximately by the sum of the covalent radii of the two atoms or Ni-N=2.00Å. The other distances used varied around this value. For the NH_3 self-consistent calculations, the H-N-H angle was kept fixed, while some N-H values around 1.00Å were taken into account.

In order to increase the variational freedom, we have extended the basis set in both molecules by including the virtual atomic orbitals (4p), (3d) and (2s,2p) for Ni, N and H respectively. In the atomic calculations a potential well trapezoid-like shaped – with a depth of -2.00 Hartrees – was added to the atomic potential so as to keep the hydrogen diffuse virtual orbitals (2s,2p) bounded. This procedure was also adopted for N, since it acquires a much larger negative charge during the self-consistent process. Moreover, the basis set was derived by considering at the same time two facts: to make it more consistent with the real molecules and to take into account that the total energy algorithm (see Eq. 6) uses as the reference system the separated atoms in the basis set, which turns it essential to fix it for each molecule. In order to define the basis set to be used the interatomic distance Ni-N=2.00Å was chosen for $NiNH_3$ and the following procedure was adopted: at the end of each convergence of the self-consistent potential a Mulliken-type population analysis is performed [5i], and the population obtained is used to define atomic charges and configuration for the Ni, N and H atoms in $NiNH_3$ molecule. For this configuration a new self-consistent atomic calculation is obtained. This procedure is stopped before achieving the optimum basis set. By an optimum basis set we mean that the configuration of the basis atomic orbitals is approximately the same as that of the atoms in the real molecule. The reason for that is that the same basis set has to be used for different interatomic distances as discussed above. To define the basis set for NH_3 an additional fact was considered: the bonding between N and H in the $NiNH_3$ and NH_3 molecules respectively for the asymptotic Ni-N values and at the equilibrium bond length has to be comparable. For this reason, the basis functions for NH_3 was determined by considering the Mulliken-

type population for the largest Ni-N distance investigated in $NiNH_3$(Ni-N=3.33Å). These populations were used to define atomic charges and configurations for the N and H atoms at the N-H=1.00Å interatomic distance in order to obtain atomic orbitals for the basis set. The remaining procedure is the one described above. It is important to emphasize that for both molecules an optimum criterion of convergence of the self-consistence potential was adopted for each interatomic distance examined. Thus, the electronic structure and, accordingly, the electronic configuration of the molecules reflect this optimizing procedure.

All the electrons were taken into account. The total number of points for the self-consistent calculations was approximately 13.500 and 18.800 for NH_3 and $NiNH_3$ respectively. However, 87% of them were generated by using a precise polynomial numerical integration inside spheres of radii equal 0.95, 0.53 and 0.26Å around Ni, N and H respectively. This procedure assures us that the core and shallow orbitals will be well described. The remaining points outside these spheres were obtained by a pseudo-random Diophantine scheme. A total of 81.000 and 114.700 points respectively for the NH_3 and $NiNH_3$ molecules were used to calculate the total energy with the same partioning of points as described before.

By using polynomial functions the best fitting was pursued in all curves presented here.

B- Ammonia

The total energy relative to an arbitrary origin for different N-H distances is plotted in Fig. 1. A and B curves refer to the self-consistent caluclations using respectively the Kohn-Sham and von Barth-Hedin potentials. A total of twelve points was considered ranging from 0.53 to 1.48Å. It is to be noted that on the whole the effect of the von Barth-Hedin correction (correction between electrons of different spins) is only to lower the total energy values. The shape and the equilibrium bond length, found to be around 1.03Å, in excellent agreement with the experimental value for H-N-H=107.2^0, are essentially the same. It is interesting to note that subtracting one curve from the other one obtains a straight line which implies a linear correlation with the N-H interatomic distances.

We have obtained $1a_1^2 2a_1^2 1e^4 3a_1^2 (^1A_1)$ for the ammonia electronic configuration in a wide range of the N-H distances studied.

The lowest energy molecular orbital belonging to the totally symmetric representation ($1a_1$) is characterized by the N1s electrons. The latter trio forms sp^3 hybrid orbitals with a tetrahedral disposition and strong directional properties. Essentially these orbitals are respectively of N2s, N2p_x/2p_y and N2p_z character. However, the overall characteristic of

this set of molecular orbitals, enveloping the eight valence electrons, is changed along the N-H series. For the shorter N-H distances the $2a_1$ orbital shows a non-negligible degree of hybridization between the dominant 2s function of N and N$2p_z$ and an admixture with H1s orbital The charge distribution (in % of one electron) for the second of them increases from 3% to approximately 16% within the range of 0.5Å <N-H<0.8Å and then it decreases continuosly reaching 3% at N-H=1.48Å, the largest interatomic distance considered. In contrast, the charge distribution for the N$2p_z$ function diminishes smoothly from 14% to 3% for distances between 0.53Å and 1.48Å. The next orbital (1e degenerate) presents considerable mixture between N$2p_x$/ $2p_y$ and H1s as expected from the C_{3v} symmetry. The degree of mixture increases rapidly and from 0.85Å to the equilibrium bond length, N-H=1.03Å, the 1e orbital is almost fifty-fifty. From this distance on the degree of bond between N and H starts dropping slowly; however, even at the largest distance considered the 1e orbital has a non-negligible contribution of H1s (34%). Finally the last occupied orbital $3a_1$ describes the nitrogen lone pair electrons ($2p_z$). Related to this feature there exists a small hybridization with N2s as well as a small H1s contribution. The predominant N$2p_z$ character is increased with interatomic distance from 78% to 90% at 1.03Å. From this point on it diminishes in a marked way until 80% at the largest N-H distance taken into account. An opposite dependence is observed for N2s presenting however, a smoother trend than the $2p_z$ function, while the H1s contribution might be certainly ignored between 0.6 and 1.2Å. Around 1.2Å it is once again observed and reaches the fractional charge contribution of 8% at the largest N-H interatomic distance.

The results discussed above are displayed graphically by the Mulliken-type bond orders (Fig. 2). There, the a_1 and e curves are the N-H bond order summed over all the occupied molecular orbitals belonging to each symmetry of the C_{3v} group and the a_1+e curve is the sum of them. Thus, for instance, the contributions coming from the 2s and $2p_z$ functions of N and H1s are simultaneously taken into account in a_1. They are derived from the self-consistent calculations considering the von Barth-Hedin potential. We may notice that the antibonding nature of the totally symmetric representation a_1 decreases with increasing N-H distances. This fact is strongly related to the reduction of the 2s-$2p_z$ degree of hybridization present in both valence orbitals a_1 and also the H1s contribution. Around N-H=0.7Å, it acquires a bonding character which in the limits of 0.7Å <N-H<1.1Å becomes more and more positive and decreases gradually slowly up to N-H=1.48Å. The degenerate orbital e, which is responsible for the largest degree of mixture between N and H, shows a bonding nature around N-H=0.65Å. This characteristic increases continuously up to N-H=0.85Å. From 0.85Å to approximatelly 1.15Å it remains virtually constant and then it increases smoothly its positive bonding character until the upper N-H interatomic

limit investigated. The resultant curve (a_1+e) is approximatelly of the same shape as e symmetry curve. However, the largest bond order value is achieved around N-H=0.90Å and it stays approximately fixed until the N-H=1.1Å interatomic distance. This fact coincides with the increasing contributions of the N2p_z and N2s respectively in the $3a_1$ and $2a_1$ orbitals and the large degree of admixture between N and H in 1e, as mentioned before. These results do not differ significantly from the ones obtained using the Kohn-Sham potential. As can be seen from the total energy curves (Fig. 1), the correlation between electrons of different spins is insignificant for the NH_3 molecule. We can explain this result taking into account the diffuse shape of the sp^3 orbitals. From this consideration it is clear why at the equilibrium distance the $3a_1$ orbital is predominantly of N2p_z character.

The N-H equilibrium bond length obtained by DVM is much closer to those calculated by other theoretical methods based on LSDA density-functional theory [6b,16a]. Becke et al have pointed out that truncated basis set in LCAO methods can be responsible for sistematic error in LSDA calculations. Becke developed a computational method, which is free of conventional LCAO basis set [6a]. Comparison between our results [6b] suggests that the errors due to basis-set truncation were largely bypassed by the procedure adopted here to mount the basis set used in our calculations.

C- $NiNH_3$

We have considered for $NiNH_3$ the configuration:
($\uparrow$) $9a_1^1 10a_1^1 4e^2 5e^2$
($\downarrow$) $4e^2 5e^2$
which yields a $^3A_1$ state. In fact, we are not particularly concerned about the actual ground state of the $NiNH_3$ molecule. However, this configuration looks especially interesting since one $3d_{z^2}$ hole is introduced by failing to take the $9a_1\downarrow$ into consideration thus minimizing the overlap between the metal $3d_{z^2}$ orbital and the lone pair N2p_z. Indeed, the ground state found for $NiNH_3^+$ is a $^2A_1$ state derived from the Ni^+ $3d^9$ occupation with a hole in the $3d_{z^2}$ orbital to minimize repulsion [3f]. However, for a more rigorous description in terms of repulsion, the 4s-$3d_{z^2}$ hybridization mechanism must be considered; it can also reduce (s-d hybrid) or increase (s+d hybrid) the metal-ligand repulsion by decreasing or increasing respectively the charge density along the Ni-N axis. Both of them will be emphasized in our discussion.

In Fig. 3 the total energy curves are plotted with respect to an arbitrary origin, using the Kohn-Sham (A) and von Barth-Hedin (B) potentials. It is important to pay attention to the energy scale: the left hand one is associated with A potential while the right hand

one refers to the B potential. We have carried out self-consistent calculations by examining ten Ni-N interatomic distances from 1.75 to 3.33Å. One observes that the dependence of the total energy on the potential employed differs from the ammonia molecule. The marked difference concerns the distinct values obtained for the equilibrium distance. They are around 1.98Å and 1.96Å for the A and B curves respectively. The regions around these values are focused in detail on Fig. 4. Calculations of diatomic molecules have shown that both Hartree-Fock-Slater (HFS), in which the correlation between electrons of different spin is not considered, and Local Density Approximation (LDA) give equilibrium distances closer to the experimental values than Hartree-Fock scheme. However, there are some examples where LDA is in better accord with experiment than HFS [16b]. As compared to the NH_3 case, the lowering energy effect related to the von Barth-Hedin correction is more strongly in $NiNH_3$ and the shape of the two curves is quite similar as illustrated in Fig. 3. It is also interesting to emphasize that contrary to the behaviour of NH_3, a subtration of one curve from the other yields two straight lines with different slopes which cross far from the equilibrium distance region, around Ni-N=2.24Å.

In Fig. 5 the total bond orders (a_1+e) of N-H, Ni-N and Ni-H obtained by self-consistent calculations with the von Barth-Hedin potential are displayed. Differences between both potential are negligible. Let us start by examining the first one.

It can be seen that the N-H curve presents a bonding character everywhere, as expected. However, this feature is more pronounced for small values of Ni-N distance and diminishes smoothly until the equilibrium region. From then on, the bonding character continues to decrease with a less monotonous behaviour and at approximately Ni-N=2.75Å it becomes constant around 0.4, comparable to the total bond order (a_1+e) value at the equilibrium bond length in ammonia (see Fig. 2). In order to extend our discussion let us introduce Fig. 6. It shows the higher energy one-electron energy levels of the NH_3 and $NiNH_3$ molecules at the equilibrium distance. It also displays the atomic valence levels of Ni, N and H obtained with atomic local density calculation. The orbitals from $7a_1$ to $8a_1$ correspond only to the NH_3 molecule. It is interesting to note that this set has lower energies than that found in the ammonia molecule. These results suggest that at the equilibrium distance (N-H=1.03Å) the NH_3 molecule in $NiNH_3$ becomes more stable than without Ni. The lower of these orbitals ($7a_1$) presents from the qualitative point of view the same composition determined for the $2a_1$ orbital in NH_3. However, it shows a reasonable degree of mixture between N2s (80%) and H1s (17%). The same characteristic is repeated in the degenerate 3e orbitals. The differences in energy between the $2a_1$ and 1e NH_3 orbitals and their respective partners in $NiNH_3$ have approximately the same values. This observation is important when the next orbital is considered. Difference in

energy between the values of the $8a_1$ orbital in $NiNH_3$ and $3a_1$ is markedly larger. The reason for this is the presence of 4s (5%) and $3d_{z^2}$ (14%) functions of Ni suggesting the formation of a 4s-$3d_{z^2}$ hybrid which reduces the charge density along the Ni-N axis and as a consequence, the repulsion [3b].

The next curve in Fig. 5 refers to the Ni-N bond order and differs significantly from the others. It shows that the antibonding character drops rapidly with the Ni-N distance. The order of the bonds are almost linearly correlated with the Ni-N interatomic values. This behaviour is present up to approximately Ni-N=2.45Å. Above this value the curve becomes smooth and a bonding character is observed which remains constant from 2.90Å on. Moreover, we can observe a marked antibonding character at Ni-N=1.96Å, the distance found to be the equilibrium bond length (see Fig. 4). This result reveals that the electronic configuration considered for the $NiNH_3$ molecule ($^3A_1$) can not give useful information us to the ground state. However, from the present point of view, the minimum energy configuration is of limited importance. Our interest here is to analyse the response of the electronic density ρ to the bonding between Ni and NH_3 in order to compare our results with those reported in the literature [3b,3f], using other theoretical methods.

The explanation of the behavior associated to the curve discussed above comes as expected fundamentally from the set of orbitals belonging to a_1 symmetry ($9a_1\uparrow$ and $10a_1\uparrow$). Firstly, let us examine the region with an antibonding character (1.7Å <Ni-N<2.5Å). Here, the orbital $9a_1\uparrow$ is essentially constituted of the valence $3d_{z^2}$ function of Ni. Its contribution for $9a_1\uparrow$ rises rapidly from approximately 66% to 93% at Ni-N=1.75Å and 2.25Å respectively. On the other hand, the contributions from the Ni4s and N$2p_z$ orbitals to $9a_1\uparrow$ present exactly the opposite behaviour. The former shows a pronounced reduction from 22% to 5% while the latter diminishes quite smoothly from approximately 4% to 1.5%. The virtual orbitals of H (2s and 2p) are also found but in a smaller fractional proportion than the others. From 2.0Å on they can be considered negligible. Within the bonding region ranging from 2.5Å to 3.1Å the charge contribution due to Ni$3d_{z^2}$ shows a monotonous correlation with Ni-N distance, but it is still positive (from 95% to 97%). At the largest interatomic value considered (Ni-N=3.33)Å, such contribution drops abruptly to 76%. This effect is compensated by a sharp increase of around 20% in the 4s function of Ni, small contributions from H2s and 2p are present once again. However, except for Ni-N=2.5Å with 2%, the Ni4s orbital shows negligible contributions for $9a_1\uparrow$ within the remaining range of bonding character, while on the contrary, the N$2p_z$ function varies continuously from 1.6% to 2.5%. In general, the highest occupied orbital in energy with a_1 symmetry ($10a_1\uparrow$) shows a fractional charge distribution pattern quite similar to $9a_1\uparrow$. However as compared with $9a_1\uparrow$ the contributions due to the orbitals $3d_{z^2}$ and 4s of Ni as

a function of Ni-N distance behave in reverse order when the virtual functions of H are substituted by Ni4p_z and N2s. Within the antibonding region (1.7Å <Ni-N<2.5Å), Ni4s rises with interatomic distance from nearly 73% to 90%. This trend continues until Ni-N=3.1Å at which distance a contribution of around 78% is observed. Such value indicates how abruptly the charge contributions drop within the short bonding range of 3.10Å <Ni-N≤ 3.33Å. An opposite behaviour is observed for the functions 3d_{z^2} and 4p_z of Ni. Both of them decrease markedly in the limit of the antibonding region and show a monotonous dependence on interatomic distances larger than 2.5Å. In % of one electron, the charge distribution of Ni3d_{z^2} and Ni4p_z vary respectively from 16.% to 1.3% between the limits of 1.75Å ≤Ni-N≤2.54Å and from 11.15% to 1.3% within the range of 1.75Å ≤Ni-N≤2.84Å. From the upper distance limits on their contributions are negligible but at Ni-N=3.33Å contributions around 11% and 7% corresponding respectively to 3d_{z^2} and 4p_z of Ni take place. The 2p_z and 2s valence orbitals of N remain essentially fixed inside the limits of the antibonding range with fractional contributions around 3.5% and 1.5% respectively. Outside this limit, the N2p_z orbital exhibits a trend similar to 3d_{z^2} and 4p_z of Ni: it drops smoothly from 3.2% to 2.4% at 3.1Å and then it rises again until 3% at 3.33Å. Contributions due to N2s are negligible within the bonding region, except for the last point examined, where 1% of this function is found.

The results discussed above suggest that more than one process, with different weights, is responsible for the appearance of the Ni-N bond order and of the total energy curves (Fig. 3). The most important of them is due to minimization of the overlap between the Ni3d_z^2 orbital and the lone pair N2p_z as a function of the distance. This effect reduces significantly the repulsion between the metal and ligand along the z axis, increasing considerably the bonding character between Ni and N. The predominance of this process in relation to the others becomes obvious when the small Ni-N values are observed. Secondly, we can also take into account the 4s-3d_{z^2} hybridization. Its influence is especially important when there exists a similar spatial extend of these orbitals as found on the left-hand side of the first-row transition metal. However, the repulsion Ni-N can be reduced by promoting one 4s electron into the compact 3d orbital. This mechanism is fundamentally present in 9a_1↑ covering all interatomic distances until Ni-N=3.1Å while 10a_1↑ shows an oppositive trend but not sufficiently different to invalidate comparisons, because the charge distributions are partitioned in a different way. For example, the contributions due to Ni3d_{z^2} in 9a_1↑ and Ni4s in 10a_1↑ rise respectively by 26% and 19% until Ni-N=3.1Å. This suggests a resultant promotion of electrons from 4s to 3d_{z^2}. In Table 1 the charges, Mulliken-type populations and magnetic moments for all the Ni-N distances considered, are given. The Ni configuration is already near $3d^9 4s^1$ at the smallest Ni-N distance and

it is $3d^{8.99}4s^{0.82}4p^{0.06}$ at the equilibrium distance (Ni-N=1.96Å). As shown in Table 1, the 3d and 4s population increases as a function of the distance. This means that the dissociation would lead to Ni $3d^9 4s^1$ (^{3}D) instead of the Ni ground state $3d^8 4s^2$ (^{3}F) [17]. In fact, for the largest Ni-N interatomic distance studied a Ni configuration $3d^9 4s^1 4p^{0.01}$ is obtained. It can be seen that the charges on Ni and N decrease smoothly along the Ni-N series except at 2.54Å, where a more pronounced variation is observed. The charge on H shows a different behaviour: it increases smoothly, however above 2.54Å this trend is reversed. The magnetic moment at Ni comes essentially from the 3d, 4s and 4p functions. As seen in Table 1 when the Ni-N distance is increased, the contributions of these orbitals converge for values which are in agreement with the $NiNH_3$ electronic configuration adopted here: spin-down $9a_1$ and $10a_1$ orbitals are not occupied. Finally, let us consider the admixture between the 4s and $4p_z$ functions which are present in the $10a_1$ orbital. This hybridization can contribute to minimize the Ni-N repulsion if the combination of the plus and minus signs of the angular lobes of the $4p_z$ function with 4s results in a polarization away from NH_3 [3f].

The last curve in Fig. 5 refers to the Ni-H bond order. The anti-bonding character is smoothly correlated to the Ni-N distances, showing a positive slope until approximately 2.6Å. From this point on the antibonding character is fixed in relation to the remaining interatomic distance values. We separate the a_1 and e symmetry from the Ni-H curve in order to discuss its behaviour. The antibonding character comes predominantly from the a_1 symmetry due to the admixture between Ni4s and H1s especially in the $8a_1$ and $9a_1$ orbitals for the small Ni-N distances. The degenerate valence orbitals 4e and 5e (Fig. 6) are respectively the Ni $3d_{xz}/3d_{yz}$ and $3d_{xy}/3d_{x^2-y^2}$ functions. Both spin up and spin down contributions are around 98.0% and 100.% along the Ni-N interatomic length series. For the shorter distances the 4e up and down orbitals exhibit some mixture with H1s. This participation is approximately 2.0% and 1.0% for both spin orientations respectively at Ni-N=1.75 and 1.88Å. From these distances on it becomes negligible. For this reason the antibonding character associated with the e symmetry decreases as a function of the distance and assumes a positive value around 2.5Å.

Conclusions

We have employed the first-principles Discrete Variational method by using the Kohn-Sham and von Barth-Hedin potentials in order to calculate the electronic structure of NH_3 and $NiNH_3$. We have examined the total energy as a function of the interatomic distances. For NH_3 an excellent agreement with the experiment was obtained for the equilibrium

distances in both potentials: 1.03Å. The Kohn-Sham and von Barth-Hedin potentials predict respectively values of 1.98Å and 1.96Å for the equilibrium bond length of $NiNH_3$ in the electronic configuration considered. The results suggest that the Discrete Variational method gives a reliable description of systems with strong directional properties. At the equilibrium distance, the resulting structure of NH_3 consists of three molecular orbitals describing the bonding between the N and H atoms and an orbital of predominantly lone pair $N2p_z$ character. The nature of the bonding of lone pair NH_3 to Ni was discussed in terms of the minimization of the overlap between the $Ni3d_{z^2}$ and $N2p_z$ functions, hybridization and the promotion of the 4s electron into the compact 3d orbital to reduce repulsion along z axis.

Acknowledgements

The author would like to thank Diana Guenzburger and D.E. Ellis for valuable constant advise. The author is also indebted to Afonso Gomes and George Bemski for their interest. Computations were carried out at the Centro Brasileiro de Pesquisas Físicas, Rio de Janeiro.

Figure Captions

Figure 1 – Total energy of NH_3 as a function of the N-H interatomic distance. The A and B curves refer respectively to the Kohn-Sham and von Barth-Hedin potentials.

Figure 2 – N-H Mulliken-type bond orders of NH_3 as function of the interatomic distance: the a_1 and e curves are the total contribution from the occupied orbitals of the C_{3v} symmetry.

Figure 3 – Total energy of $NiNH_3$ as a function of the Ni-N interatomic distance. The A and B curves are associated respectively with the Kohn-Sham and von Barth-Hedin potentials on different vertical scales.

Figure 4 – Total energy of $NiNH_3$ versus Ni-N distance (Fig. 3) enlarged to show details.

Figure 5 – The total N-H, Ni-N and Ni-H (a_1+e) Mulliken-type bond orders versus Ni-N interatomic distance.

Figure 6 – Valence one-electron energy level schemes for $NiNH_3$ and NH_3 at the equilibrium distances. Atomic levels of neutral Ni and N are also shown.

Table Caption

Table 1 – Ni-N interatomic distances, charges, magnetic moments (spin-up minus spin-down populations) and populations for $NiNH_3$.

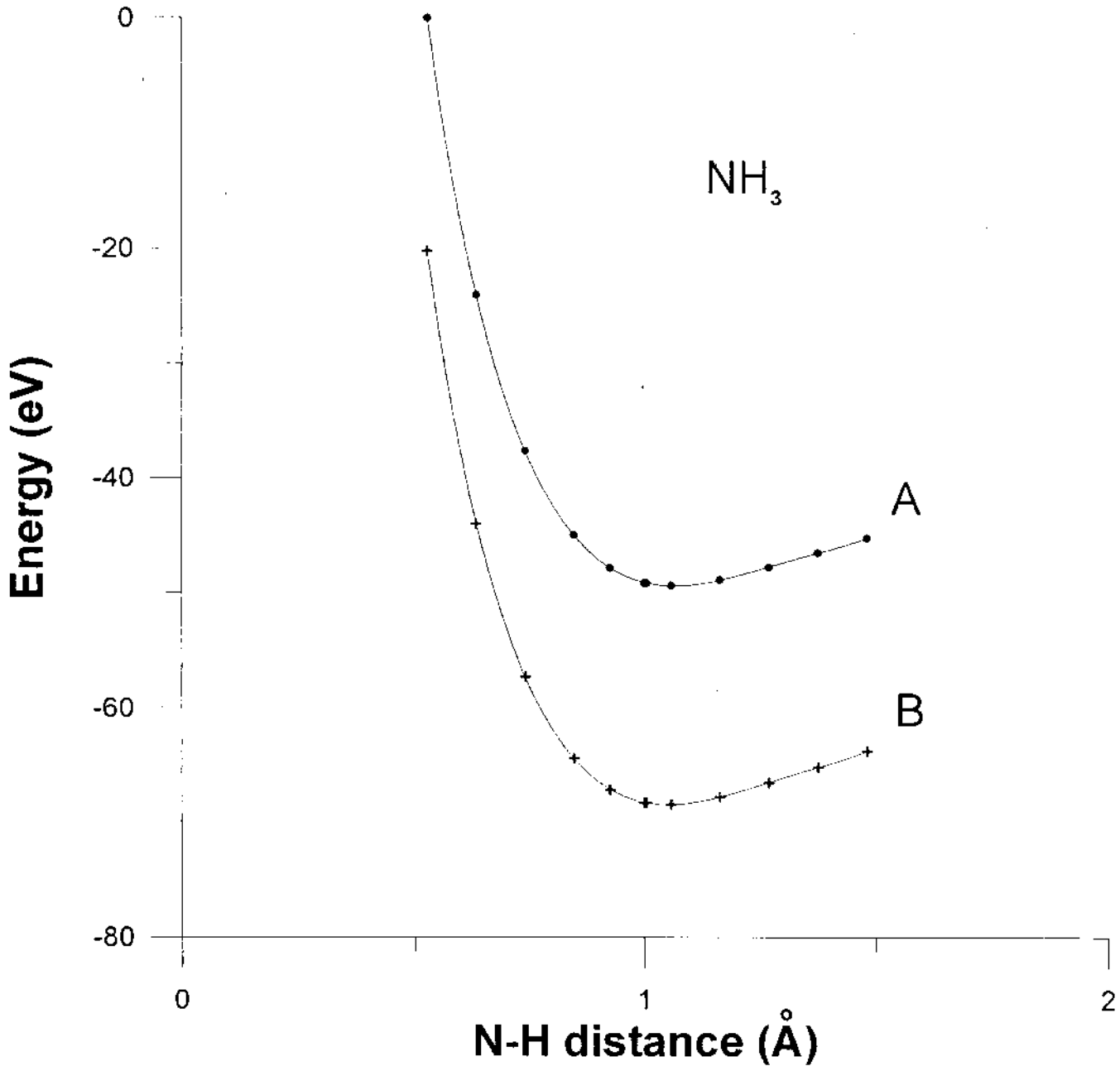

Fig. 1

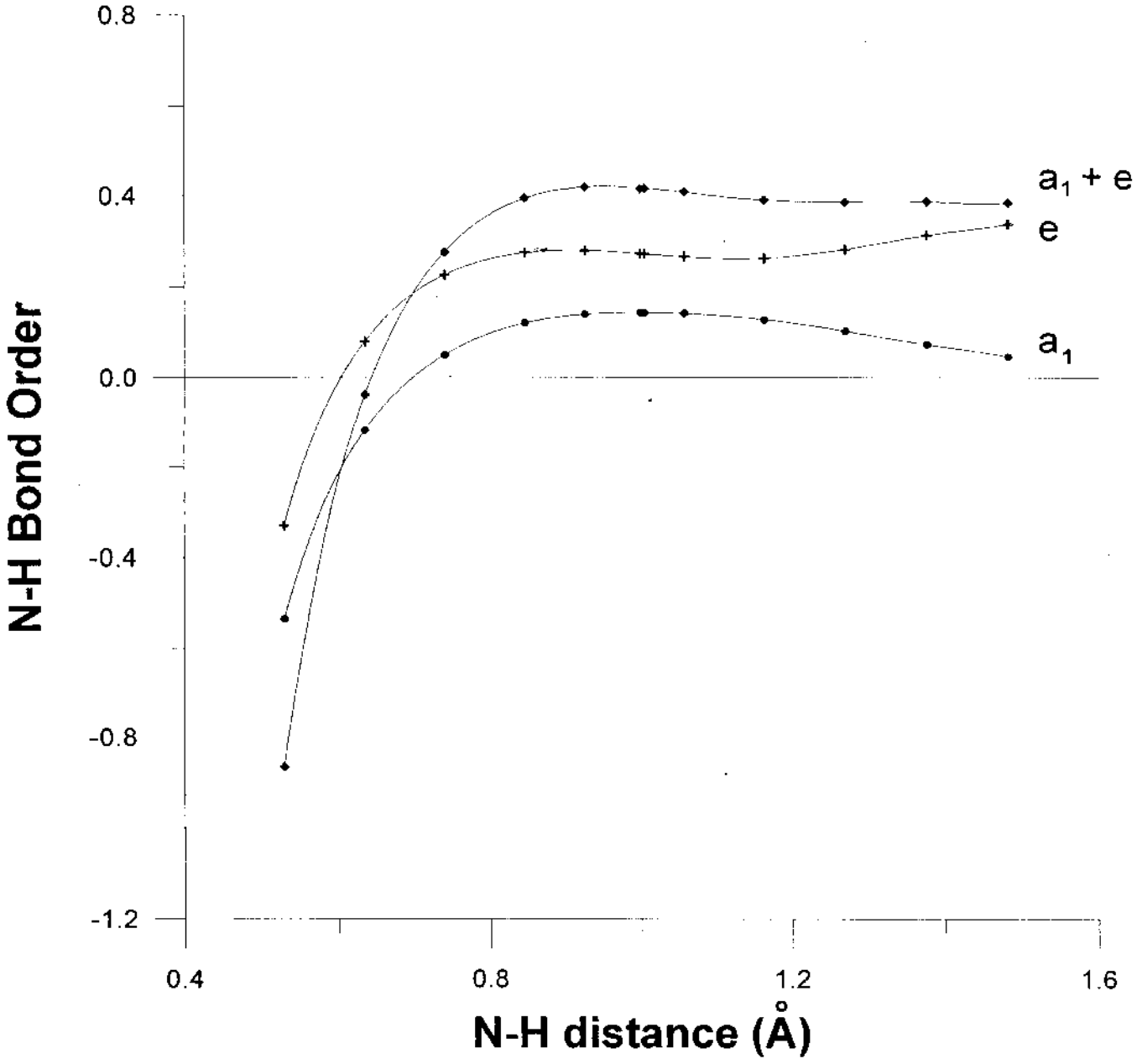

Fig. 2

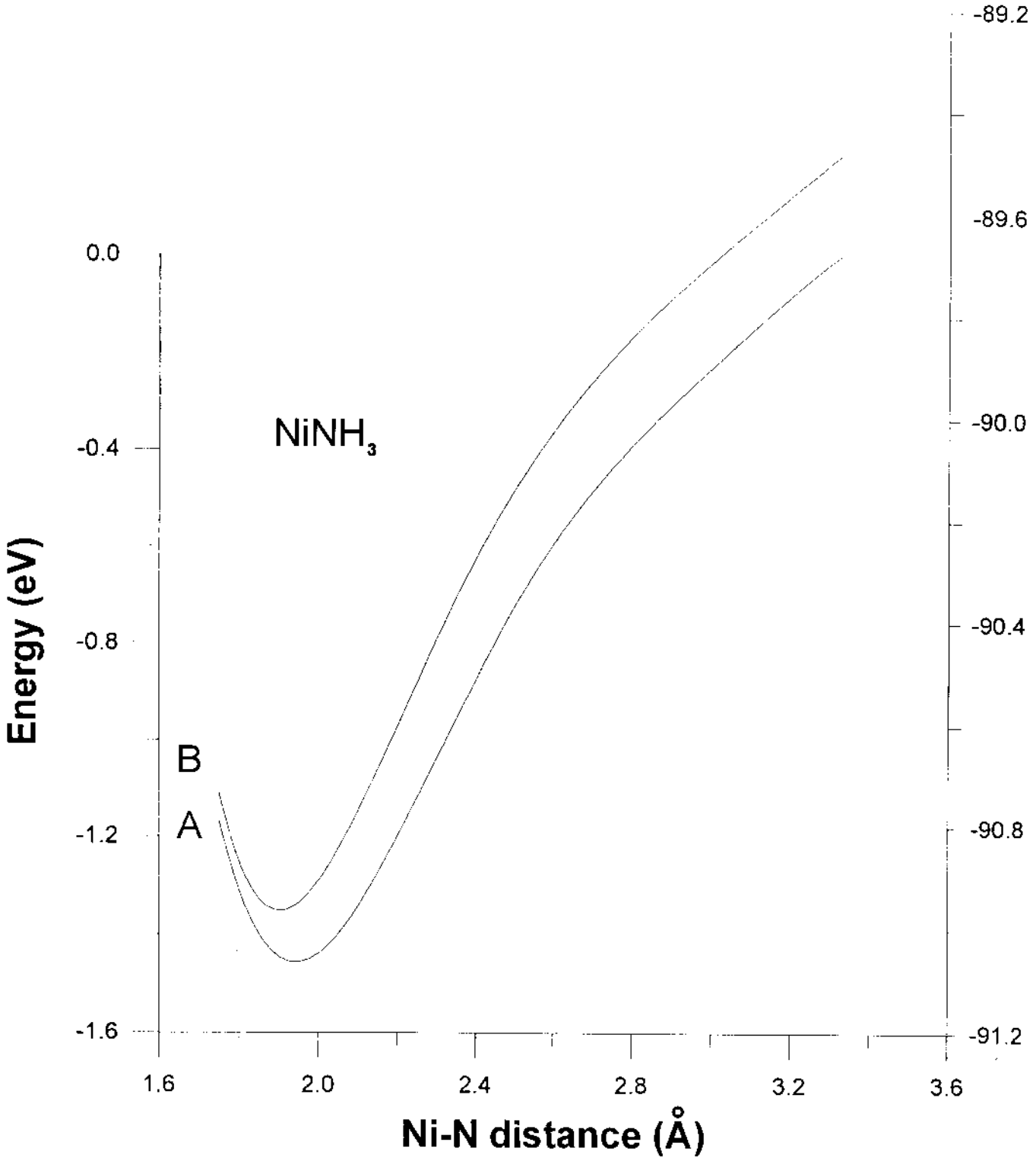
-89.2
-89.6
-90.0
-90.4
-90.8
-91.2
0.0
-0.4
-0.8
-1.2
-1.6
NiNH3
B
A
Energy (eV)
1.6
2.0
2.4
2.8
3.2
3.6
Ni-N distance (Å)

Fig. 3

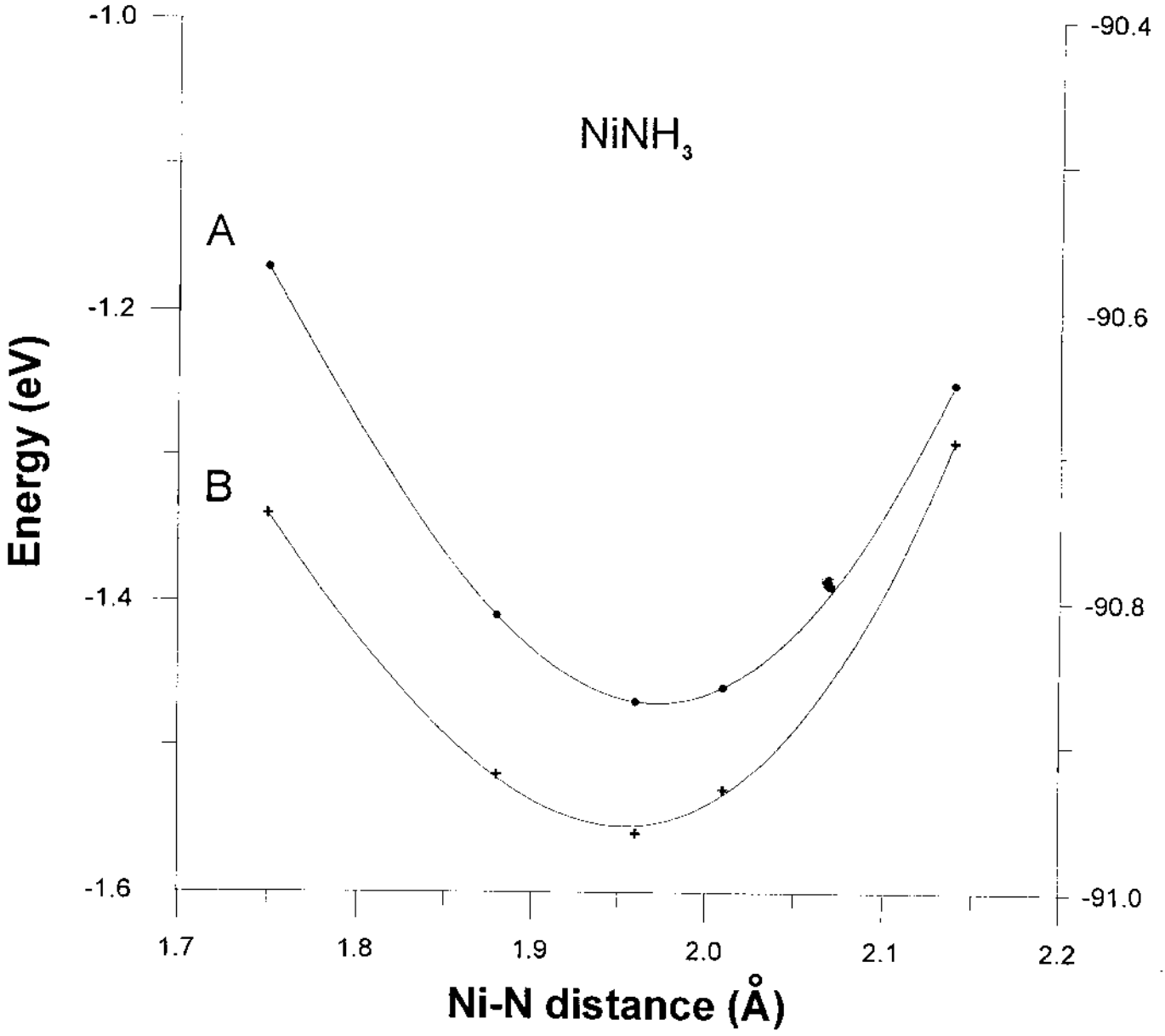
NiNH3
A
B
Energy (eV)
-1.0
-1.2
-1.4
-1.6
-90.4
-90.6
-90.8
-91.0
1.7
1.8
1.9
2.0
2.1
2.2
Ni-N distance (Å)

Fig. 4

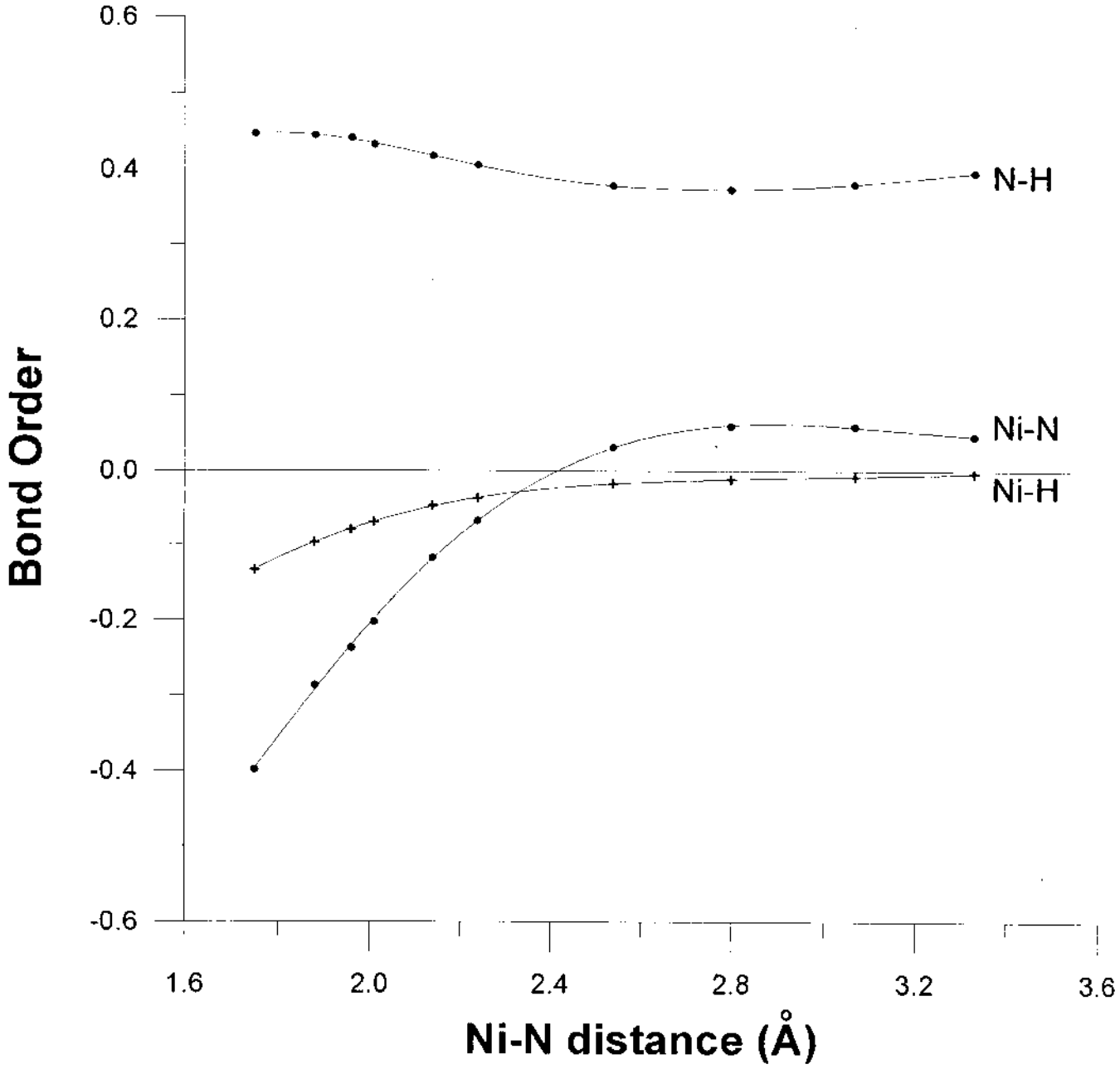
0.6
0.4
0.2
0.0
-0.2
-0.4
-0.6
Bond Order
N-H
Ni-N
Ni-H
1.6
2.0
2.4
2.8
3.2
3.6
Ni-N distance (Å)

Fig. 5

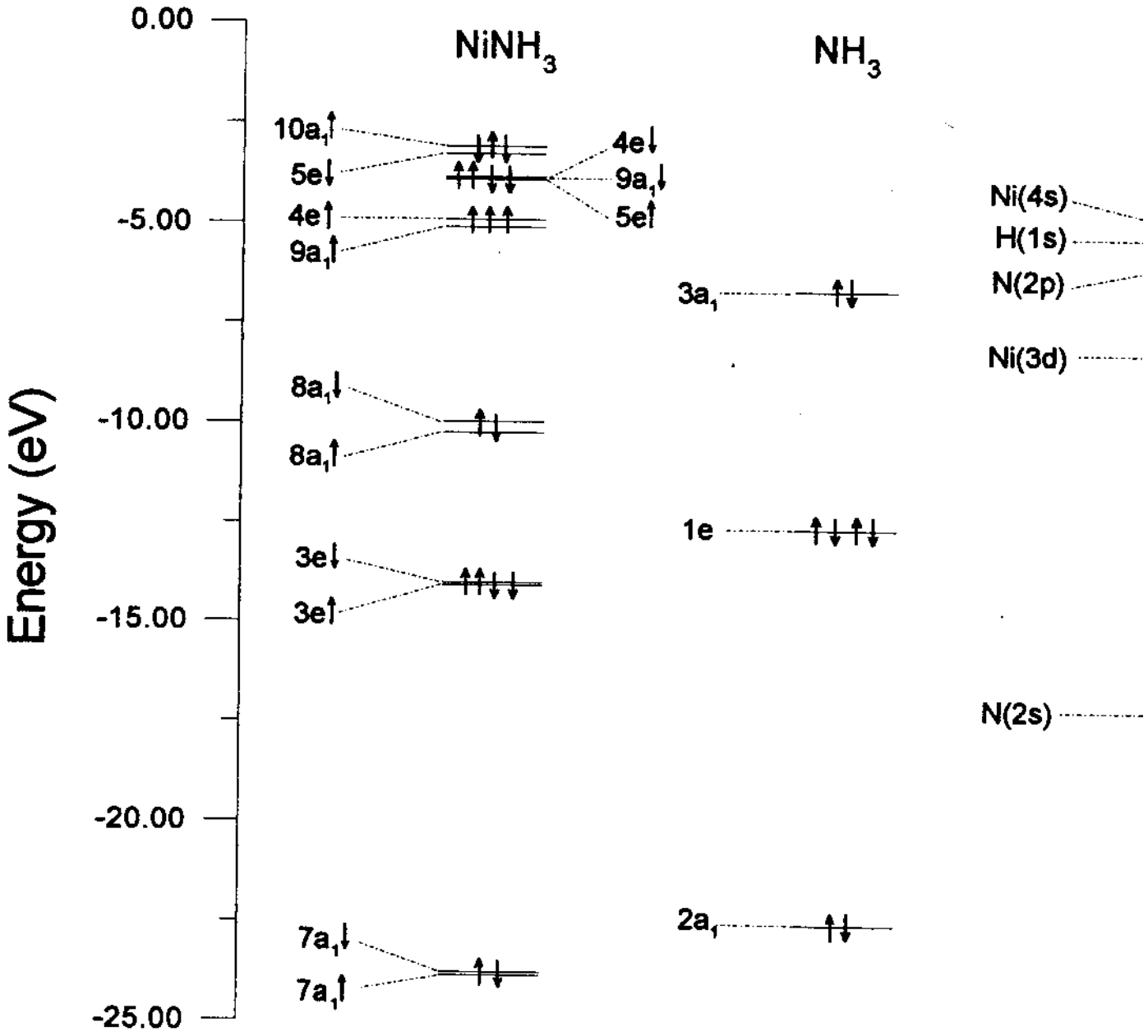
0.00
-5.00
-10.00
-15.00
-20.00
-25.00
Energy (eV)
NiNH3
NH3
10a1↑
5e↓
4e↑
9a1↑
4e↓
9a1↓
5e↑
8a1↓
8a1↑
3e↓
3e↑
7a1↓
7a1↑
3a1
1e
2a1
Ni(4s)
H(1s)
N(2p)
Ni(3d)
N(2s)

Fig. 6

Ni-N (Å)	Charge			Magnetic moment (μ_B)		Ni populations		Ni orbital moments (μ_B)
	Ni	N	H	Ni	N			
1.75	+0.24	-1.26	+0.34	+1.67	+0.23	3d	8.97	+0.87
						4s	0.74	+0.73
						4p	0.09	+0.09
1.88	+0.18	-1.23	+0.35	+1.74	+0.18	3d	8.98	+0.90
						4s	0.79	+0.78
						4p	0.07	+0.07
1.96	+0.15	-1.23	+0.36	+1.78	+0.17	3d	8.99	+0.92
						4s	0.82	+0.81
						4p	0.06	+0.06
2.01	+0.13	-1.21	+0.36	+1.80	+0.15	3d	8.99	+0.93
						4s	0.84	+0.83
						4p	0.05	+0.05
2.14	+0.09	-1.20	+0.37	+1.85	+0.13	3d	9.00	+0.95
						4s	0.88	+0.87
						4p	0.05	+0.04
2.24	+0.06	-1.17	+0.37	+1.88	+0.11	3d	9.00	+0.96
						4s	0.90	+0.89
						4p	0.04	+0.03
2.54	+0.01	-1.09	+0.36	+1.94	+0.07	3d	9.01	+0.98
						4s	0.96	+0.94
						4p	0.03	+0.02
2.80	-0.01	-1.07	+0.36	+1.96	+0.04	3d	9.01	+0.99
						4s	0.99	+0.96
						4p	0.02	+0.01
3.07	-0.01	-1.04	+0.35	+1.97	+0.03	3d	9.01	+0.99
						4s	1.00	+0.97
						4p	0.01	+0.01
3.33	-0.01	-1.01	+0.34	+1.98	+0.02	3d	9.00	+0.99
						4s	1.00	+0.98
						4p	0.01	+0.01

Table 1

References

[1] (a) P.S. Bagus, K. Hermann and C.W. Bauschlicher, Jr., Chem. Phys. 81 (1994) 1966.
(b) C.W. Bauschlicher, Jr., Chem. Phys. 83 (1985) 2619.

[2] (a) K. Hermann and P.S. Bagus, Phys. Rev. B28 (1983) 560.
(b) P.S. Bagus, K. Hermann and C.W. Bauschlicher, Jr., Chem. Phys. 80 (1984) 4378.
(c) K. Hermann, P.S. Bagus and C.W. Bauschlicher, Jr., Phys. Rev. B 31 (1985) 6371.
(d) C.W. Bauschlicher, Jr., Chem. Phys. 83 (1985) 3129.

[3] (a) M.R.A. Blomberg, U.B. Brandemark, P.E.M. Siegbahn, K.B. Mathisen and G. Karlström, J. Phys. Chem. 89 (1985) 2171.
(b) C.W. Bauschlicher, Jr., Chem. Phys. 84 (1986) 260.
(c) C.W. Bauschlicher, Jr., P.S. Bagus, C.J. Nelin and B.O. Roos, J. Chem. Phys. 85 (1986) 354.
(d) M. Rosi and C.W. Bauschlicher, Jr., Chem. Phys. 90 (1989) 7264.
(e) M. Rosi and C.W. Bauschlicher, Jr., Chem. Phys. 92 (1990) 1876.
(f) S.R. Langhoff, C.W. Bauschlicher, Jr., H. Partridge and M. Sodupe, J. Phys. Chem. 95 (1991) 10677.
(g) M. Sodupe, C.W. Bauschlicher, Jr., S.R. Langhoff and H. Partridge, J. Phys. Chem. 96 (1992) 2118.
(h) C.W. Bauschlicher, Jr., H. Partridge and S.R. Lanaghoff, J. Phys. Chem. 96 (1992) 2475, 3273.

[4] (a) D.E. Ellis and G.S. Painter, Phys. Rev. B2 (1970) 2887.
(b) D.E. Ellis, Int. J. Quant. Chem. S2 (1968) 35.
(c) E.J. Baerends, D.E. Ellis and P. Ros, Chem. Phys. 2 (1973) 41.

[5] (a) D. Guenzburger and D.E. Ellis, Phys. Rev. B31 (1985) 93.
(b) M.R. Press and D.E. Ellis, Phys. Rev. B35 (1987) 4438.
(c) P.K. Khowash and D.E. Ellis, Phys. Rev. B39 (1989) 1908
(d) J. Terra and D. Guenzburger, Phys. Rev. B44 (1991) 8584.
(e) J. Guo, D.E. Ellis and D.J. Lam, Phys. Rev. B45 (1992) 13647.
(f) D. Guenzburger and D.E. Ellis, Phys. Rev. B45 (1992) 285.
(g) D.E. Ellis, E.B. Saitovitch and D.J. Lam, Physica C 198 (1992) 57.
(h) D. Guenzburger, R.R. Sobral and A.P. Guimarães, J. Phys.: Condens. Matter 6

(1994) 2385.
(i) D.E. Ellis, J. Guo and J.J. Low, Quantum Chemistry Approaches to Chemisorption and Heterogeneous Catalysis, Ed.: F. Ruette, Kluwer Academic Publishers, Netherlands (1992).

[6] (a) A.D. Becke, J. Chem. Phys. 84 (1986) 4524.
(b) R.M. Dickson and A.D. Becke, J. Chem. Phys. 99 (1993) 3898.

[7] J. Terra and D. Guenzburger, unpublished.

[8] E.B. Saitovitch, J. Terra and F.J. Litterst, Phys. Rev. B 39 (1989) 6403.

[9] S. Lundquist and N.H. March, Theory of the Inhomogeneous Electron Gas, Plenum, New York, 1970, p. 79.

[10] R.G. Parr and W. Yang, Density-Functional Theory of Atoms and Molecules, Oxford University Press, New York, 1989.

[11] U. von Barth and L. Hedin, J. Phys. C5 (1972) 1629.

[12] B. Delley and D.E. Ellis, J. Chem. Phys. 76 (1982) 1949.

[13] A. Rosén, D.E. Ellis, H. Adachi and F.W. Averill, J. Chem. Phys. 65 (1976) 3629.

[14] B. Delley, D.E. Ellis, A.J. Freeman, E.J. Baerends and D. Post, Phys. Rev. B27 (1983) 2132.

[15] G. Herzberg, Electronic Spectra of Polyatomic Molecules, Van Nostrand Reinhold, New York, 1966.

[16] (a) L. Fan and T. Ziegler, J. Chem. Phys. 95 (1991) 7401.
(b) T. Ziegler, Chem. Rev. 91 (1991) 651.

[17] C.E. Moore, Atomic Energy Levels, US Natl. Bur. Stand. (US) 1952, p. 97.